PROCEEDINGS OF SCIENCE

Heavy quarks at finite temperature

Johannes Heinrich Weber[a,*]

[a] *Institut für Physik & IRIS Adlershof & RTG 2575, Humboldt-Universität zu Berlin, D-12489 Berlin, Germany*

E-mail: johannes.weber@physik.hu-berlin.de

New incarnations of heavy-ion collision experiments are turning our attention to hard processes and a more fine-grained resolution of the QGP. In this endeavor quarkonia or open heavy flavors turn out to be versatile probes, which are usually described through models based on perturbative QCD, AdS, and effective field theories. The lattice provides nonperturbative input and constraints to such models.
In-medium bottomonia, the complex static quark-antiquark potential, and the heavy-quark momentum diffusion coefficient are key quantities where lattice gauge theory has recently achieved significant progress with impact for heavy-ion phenomenology. We review these lattice results, relate them to phenomenological applications, and close with an outlook.

The 38th International Symposium on Lattice Field Theory, LATTICE2021 26th-30th July, 2021 Zoom/Gather@Massachusetts Institute of Technology

*Speaker

PoS(LATTICE2021)014

1. Introduction

Both the asymptotic freedom at short distances, where the weak-coupling approach applies, as well as a wide range of strictly non-perturbative, mutually interrelated long-distance phenomena are well-established in experimental and theoretical studies of nuclear matter (see, e.g., Refs. [1–4] for a review). On the one hand, the asymptotic freedom predicts that nuclear matter can be understood at very high temperatures or densities as a hot plasma of its fundamental partons, which are interacting weakly [5]. This high-temperature state of nuclear matter is called the quark-gluon plasma (QGP), whose properties are determined by the interplay of its scales – the temperature T, the Debye mass $m_D \sim gT$, and the magnetic scale g^2T – which are hierarchically ordered as $g^2T \ll m_D \ll \pi T$ in the strict weak-coupling limit. On the other hand, the infrared regime of nuclear matter at sufficiently low temperatures and densities can be described to a good approximation as a gas of essentially non-interacting hadrons and resonances exhibiting their respective non-perturbative vacuum properties [6]. This low-temperature state of nuclear matter is called a hadron gas. As a description in terms of a hadron gas would lead to exponential growth in the density of states, it must eventually break down at high temperatures [7].

Instead, the properties of nuclear matter and the nature of its degrees of freedom undergo dramatic transitions when its temperature is increased towards and beyond certain thresholds that depend strongly on the details of the particle content, in particular on the number and mass of the light quark flavors [8]. On the one hand, the transition in the physical world, dominated by the nearby chiral transition at $T_\chi \approx 132\,\text{MeV}$ for $N_f = 2$ massless flavors and a physical strange quark [9], is a smooth and broad crossover centered at the pseudocritical temperature of $T_\text{pc} \approx 157\,\text{MeV}$ with an uncertainty of about 1% [10, 11]. On the other hand, in the SU(3) pure gauge theory the deconfinement transition at $T_d \approx 270\,\text{MeV}$ is the relevant threshold. Not too far above those respective thresholds, i.e. up to $T \sim 300\,\text{MeV}$, the corresponding thermal medium produced in heavy-ion collisions behaves as an almost inviscid, nearly perfect fluid, which indicates a strongly-coupled medium, while quite a few of its properties become quantitatively similar to predictions from the weak-coupling expansion at $T > 300\,\text{MeV}$, e.g., heavy quark-antiquark free energies in the static limit [4, 12]. At present, how and when this thermal medium becomes weakly coupled are unsolved questions, which are addressed in ongoing research.

Heavy quarks, either considered as isolated partons or within a heavy quark-antiquark pair, are almost ideal probes for the properties of the strong interactions (see, e.g., Refs. [13, 14] for recent reviews). The former can be treated in many realistic scenarios as slowly-moving, non-relativistic probes with $m_h v \ll m_h$ in the fundamental representation of the gauge group, for whom particle-antiparticle creation and annihilation is strongly suppressed. When immersed into a thermal medium, the heavy quark primarily interacts with the medium through collisional or radiative processes. Both kinds of processes contribute to *transport phenomena*, namely they modify the energy and momentum, and thereby position of the heavy quark. The latter form non-relativistic bound states in QCD with $m_h v^2 \ll m_h v \ll m_h$. The low-lying ones have most of their support within the Coulomb core of the QCD static potential, and thereby constitute the QCD analog of positronium. Due to this analogy these bound states are called *quarkonia*. The effective field theory ideally suited to describing these bound states is potential non-relativistic QCD (pNRQCD), which is obtained by successively integrating out the scales m_h and $m_h v \sim 1/r$

(see, e.g., Ref. [15] for a review). When immersed into a thermal medium, the heavy quarkonia primarily interact with the medium through dissociative processes leading to thermal broadening, or acquire a thermal mass shift that is attributed to a screening of color charges. Due to the dissociative processes the heavy quark and antiquark may spend considerable time in a dissociated state before recombining again. Hence, a full dynamical description of in-medium quarkonia must account for the transport phenomena that govern the evolution of the dissociated state, too. The phenomena affecting both types of heavy-quark probes are due to dynamical processes, and therefore require a real-time formalism to explicitly manifest in correlation functions.

Due to the large value of the heavy-quark mass m_h, which is much larger than the emergent scale Λ_{QCD}, at which non-perturbative effects dominate, the weak-coupling approach is applicable to many analytic calculations of properties of heavy-quark systems. While the heavy-quark mass m_h is still much larger than the medium temperature T, in-medium heavy-quark systems show some resilience against thermalization. Many interactions between the heavy-quark system and its thermal environment may be considered as perturbations of vacuum-like properties that are suppressed by powers of the ratio of the scales T/m_h, even for a strongly-coupled medium. The question, which type of medium interaction or thermal perturbation is most relevant strongly depends on the regime determined by the various scales of the problem. The process of quarkonia fully thermalizing with the medium is termed *melting* independent of the underlying mechanism.

The idea of studying the thermal modification of heavy quarkonia in a heavy-ion collision is an old one. Starting from a confining potential model for the binding of J/Ψ and the Yukawa-type modification due to the Debye screening of chromoelectric fields in a QGP, Matsui and Satz deduced that quarkonia cannot survive as bound states once the thermal screening length $1/m_D$ becomes as small as the average radius $r_{\mathrm{J}/\Psi}$ [16]. They concluded that the modification of the quarkonia rates would be a fingerprint of QGP formation. Later on, these ideas were extended to the notion of sequential melting, namely, that excited quarkonia with weaker binding, and thus larger radii, would already melt at lower temperatures, thereby establishing the notion that a variety of quarkonia constitutes a thermometer of QGP [17]. Melting temperatures of different quarkonia species significantly depend in model calculations on the assumption whether the underlying potential is of a weak- or strong-binding type, where the former would be screened similar to the quark-antiquark free energies [4, 12], while the latter would retain a robust remnant of the confining interaction. The former would imply the melting of J/Ψ slightly above the crossover and of $\Upsilon(1\mathrm{S})$ around $T \sim 300\,\mathrm{MeV}$, while the latter might permit J/Ψ surviving up to significantly higher temperatures and $\Upsilon(1\mathrm{S})$ up to $T \sim 450\,\mathrm{MeV}$ [1].

Heavy-quark transport has been considered for a similarly long time. Early calculations in perturbative QCD predicted large values of the heavy-quark diffusion constant D [18], while lattice calculations in the quenched approximation [19–22] or heavy-ion phenomenology [23] seem to prefer a smaller value consistent with a strongly-coupled medium. Similarly, since effective field theory calculations [24] indicate in the hadron gas phase a decrease towards the crossover, the heavy-quark transport coefficients seem to approach in the crossover region global extrema close to the bounds predicted by the AdS/CFT correspondence, i.e. $D(2\pi T) \simeq 1$ [25]. Yet a first-principles calculation that also accounts for dynamical quarks in the crossover region is not available yet.

In heavy-ion collisions heavy quark-antiquark pairs are produced in hard processes taking place during the earliest stages. If the temperature is sufficiently high, namely $\pi T \gtrsim m_c$, which is reached

beyond $T \gtrsim 300\,\mathrm{MeV}$, then charm quark-antiquark pairs can be created from the thermal medium as well, and contribute to the bulk properties, such as the equation of state. Their total number is conserved, since the time scale of their flavor-changing electroweak decays exceeds the lifetime of the primordial fireball. Hence, heavy-quark, and more specifically, bottom-quark observables probe all stages of the collision, and provide almost unique access to its early-time dynamics, and feature prominently in the long-term planning of many heavy-ion experiments (see e.g. [1]). Description of in-medium heavy-quark evolution usually relies on perturbative QCD, effective field theory or models. All of these require some form of non-perturbative input, in particular for the strongly-coupled medium at temperatures not too far above the crossover. In many cases this input can be provided either by a suitable comparison to experimental data or by first-principles lattice gauge theory simulations. The most technically challenging aspect of such a lattice computation is that it provides Euclidean-time correlators $G(\tau, T)$ that are related to a spectral function $\rho(\omega, T)$ encoding the underlying real-time dynamics through an integral transform (in the following $\beta = {}^1/_T$),

$$G(\tau, T) = \int_{-0}^{+\infty} \frac{d\omega}{\omega} K(\omega, \tau, \beta)\rho(\omega, T), \tag{1}$$

where the kernel $K(\omega, \tau, \beta)$ has – for relativistic quarks – its own temperature dependence:

$$K(\omega, \tau, \beta) = \frac{\cosh \omega\,(\tau - {}^\beta/_2)}{\sinh {}^{\omega\beta}/_2}. \tag{2}$$

Due to the kernel's symmetry under $\tau \to \beta - \tau$ in Eq. (2), the effective number of data in $G(\tau, T)$ providing independent information on $\rho(\omega, T)$ is further reduced. So far, the inverse problem in Eq. (1) has not been solved in any case of interest without including additional assumptions or limitations that may have significant impact on the solution.

In these proceedings, we review the recent advances in lattice gauge theory with respect to the non-pertubative calculation of in-medium heavy-quark observables at finite temperature. In Section 2 we discuss heavy-quark transport, while we address heavy quarkiona in Section 3. We close with a summary and outlook in Section 4.

2. Heavy-quark transport

In the vacuum, open heavy flavors either play a role as hard partonic jets at short distances, or in the form of bound states with light degrees of freedom at long distances. Heavy-light mesons constitute the ground states of such systems. In QGP, open heavy flavors may arise either from the eventual melting of in-medium heavy quarkonia, or by not binding into a color-singlet state in the first place. In the following we focus on slowly-moving, non-relativistic heavy quarks, for whom collisional medium interactions are dominant. The screening of forces between color charges implies that these isolated heavy quarks may propagate through the medium without having to form bound states, and eventually thermalize with the environment. Due to the equipartition theorem, they possess kinetic energy $E = {}^{p^2}/_{2m_h} \sim T$ and thereby spatial momentum $\sqrt{\boldsymbol{p}^2} \sim \sqrt{m_h T} \gg T$. Successive collisions do not change the momentum $\boldsymbol{p}$ significantly and can be considered as independent kicks of $\Delta p_i \sim T$; for this reason the heavy quarks undergo Langevin-type evolution

$$\frac{dp_i}{dt} = \eta_D p_i + \xi_i(t), \quad \langle \xi_i(t_0)\xi_j(t_1)\rangle = \kappa\delta_{ij}\delta(t_0 - t_1), \tag{3}$$

where the drag coefficient η_D and the *heavy-quark momentum diffusion coefficient* κ are related on general thermodynamic grounds by the fluctuation-dissipation theorem as $\eta_D = \kappa/2m_h T$. The heavy-quark diffusion constant $D = 2T^2/\kappa$ is related to κ as well. Hence, knowledge of either η_D, κ or D is sufficient to fix the equations governing the Langevin dynamics of in-medium heavy quarks up to corrections of order T/m_h [26].

In practice, the path of least resistance is to compute κ in lattice gauge theory simulations. While it could be determined in principle through a Kubo relation from the divergence of the transport peak of the spectral function underlying the heavy-quark vector correlator at zero frequency, this is notoriously hard to compute. It was realized that a suitable heavy-quark vector correlator

$$\kappa = \lim_{\omega\to 0}\lim_{m_h\to\infty}\kappa^{(m_h)}(\omega), \quad \kappa^{(m_h)}(\omega) = \frac{1}{3\chi}\int_{-\infty}^{+\infty} dt e^{\mathrm{i}\omega t}\int d^3x \left\langle \frac{1}{2}\left\{\mathcal{F}^i(\boldsymbol{x},t), \mathcal{F}^i(\mathbf{o},0)\right\}\right\rangle, \tag{4}$$

with $\mathcal{F}^i(\boldsymbol{x},t) \equiv m_h\partial_t J^i(\boldsymbol{x},t)$, $J^i(\boldsymbol{x},t) = \bar{\psi}(\boldsymbol{x},t)\gamma^i\psi(\boldsymbol{x},t)$, and the quark number susceptibility $\chi = \beta\int d^3x \left\langle \frac{1}{2}\left\{J^0(\boldsymbol{x},t), J^0(\mathbf{o},0)\right\}\right\rangle$, reduces – after integrating out the heavy-quark fields – to a chromoelectric field-strength correlator in Euclidean time [27]

$$G_{E,R}(\tau,T) = -\frac{1}{3}\sum_{i=1}^{3}\frac{\langle \mathrm{Re\,Tr} U(\beta,\tau) gE_i(\tau,\mathbf{o}) U(\tau,0) gE_i(0,\mathbf{o})\rangle}{\langle \mathrm{Re\,Tr} U(\beta,0)\rangle}, \tag{5}$$

which is amenable to the lattice evaluation. $P = \langle \mathrm{Re\,Tr} U(\beta,0)\rangle$ is the trace of the Polyakov loop. Since such gluonic operators are very noisy quantities, efficient noise suppression techniques are indispensable for their calculation. Employing multi-level algorithms in the quenched approximation $G_{E,R}(\tau,T)$ has been obtained on the lattice by various groups in the past [19–22]. As this correlator requires multiplicative renormalization, which is to date known at the one-loop level [28], estimates of the renormalization factor had been obtained earlier using tadpole factors. After obtaining the continuum limit of the chromoelectric correlator in Eq. (5), it can be related through the kernel $K(\omega,\tau,\beta)$ in Eq. (2) to the spectral function via

$$G_{E,R}(\tau,T) = \int_{-0}^{+\infty}\frac{d\omega}{\pi}K(\omega,\tau,\beta)\rho(\omega,T), \quad \kappa = \lim_{\omega\to 0}\frac{2T\rho(\omega,T)}{\omega}. \tag{6}$$

In practice, the inverse problem in Eq. (6) is solved using models for the spectral function that enforce the known limiting behaviors in the IR and in the UV.

Novel lattice calculations have improved this situation considerably. The key ingredient to these new approaches is the use of the gradient flow instead of the multi-level algorithm for the noise reduction. The Yang-Mills gradient flow evolves the gauge fields along a fictitious fifth direction termed *flow time* τ_F [29]. The flowed fields are defined via

$$\frac{\partial V_\mu(x,\tau_F)}{\partial \tau_F} = D_\nu G_{\nu\mu}, \quad V_\mu(x,\tau_F=0) \equiv U_\mu(x), \tag{7}$$

$$D_\mu V_\nu(x,\tau_F) \equiv \partial_\mu + [V_\mu(x,\tau_F), V_\nu(x,\tau_F)], \tag{8}$$

$$G_{\nu\mu}(x,\tau_F) \equiv \partial_\mu V_\nu(x,\tau_F) - \partial_\nu V_\mu(x,\tau_F) + [V_\mu(x,\tau_F), V_\nu(x,\tau_F)], \tag{9}$$

where the discretization in Eq. (9) does not have to coincide with the discretization used in the action. Any composite local operator computed from the fields $V_\mu(x,\tau_F)$ at large enough finite flow time yields in the zero flow-time limit a linear combination of renormalized operators within the same representation,

$$\lim_{\tau_F\to 0} O[V_\mu(x,\tau_F)] = \sum_i c_i(\tau_F) O_i^{\mathrm{R}}(x). \tag{10}$$

Hence, in practice the chromoelectric correlator defined in Eq. (5) is computed using fields $V_\mu(x,\tau_F)$ at a wide enough range of flow times τ_F for different lattice spacings. Then $O[V_\mu(x,\tau_F)]$ is extrapolated to the continuum limit at each value τ_F of fixed flow time. These continuum results are extrapolated to zero flow time in an ensuing step. While the functional form of the continuum extrapolation is well motivated by the Symanzik effective theory, the details of the zero flow-time extrapolation are often somewhat ad hoc. Nonetheless, since varying the choice of the flow action in Eq. (9) permits changing the details of the finite flow-time artifacts and change the slope (and higher order τ_F dependence), these latter extrapolations appear to be usually well under control.

If the initial operator was chosen such that it cannot mix with other operators, the renormalized continuum result is obtained. While the comparison of the renormalized continuum results obtained via gradient flow, or via multi-level algorithm with one-loop renormalization factor suggests small differences between the renormalization factors, the overall time and temperature dependence of these correlators is in good agreement given the quoted errors [30, 31]. Obviously, the need for modeling the spectral functions to solve the inverse problem in Eq. (6) is not significantly affected by the change of the lattice setup used to obtain the Euclidean correlator in the continuum limit. The most recent results for κ are quantitatively consistent, albeit still with substantial uncertainties.

The use of gradient flow for computing the heavy-quark transport coefficients opens up two new windows of opportunity. The first and most obvious one is that the gradient flow as a means for noise reduction is applicable in full QCD as well, while the multi-level algorithm is not due to the non-local nature of the fermion determinant. Hence, we may expect the first calculations of the heavy-quark momentum diffusion coefficient κ in full QCD in the near future. The second and more subtle one is that the gradient flow as a means for renormalization permits to compute full chromoelectric or chromomagnetic correlation functions, such as

$$G_B(\tau,T) = \int d^3x \frac{\langle \mathrm{tr}\, U(\beta;\tau) B_i(\tau) U(\tau;0) B_i(0)\rangle}{3P}, \tag{11}$$

$$G_E(\tau,T) = \int d^3x \frac{\langle \mathrm{tr}\, U(\beta;\tau) E_i(\tau) U(\tau;0) E_i(0)\rangle}{3P}, \tag{12}$$

for which the renormalization with other means is still an unsolved problem. The real part of the chromomagnetic correlator in Eq. (11) is related to the $O(T/m_h)$ corrections to κ. Preliminary results of the first such calculations have been reported at this conference [31, 32]. The imaginary part in Eq. (12) is related to γ, the dispersive counterpart of κ, which is related to the thermal mass shift of quarkonia in pNRQCD [33].

3. Heavy quarkonia

3.1 General features

In the vacuum, quarkonia are among the most simple bound state problems of QCD. The heavy-quark mass m_h is by far the largest scale in the problem. By integrating out m_h (in terms of a Foldy-Wouthuysen transform similar to the textbook-level one used in the relativistic treatment of hydrogen) one arrives at the effective field theory of non-relativistic QCD (NRQCD) [34], which is valid at the soft scale of typical momenta $p \sim m_h v \ll m_h$. The heavy-quark or antiquark fields are described as two separate 2-component Pauli spinors, while heavy quark-antiquark pair creation and annihilation is realized through four-fermion interactions suppressed by the ratio of the scales, i.e. the heavy-quark velocity $v = p/m_h$, which is of the order of the strong coupling constant $v \sim \alpha_s(m_h)$.

For a heavy quark-antiquark pair, it is possible to further simplify the problem. Since their low-lying bound states are compact objects, a multipole expansion in the relative coordinate between quark and antiquark can be applied. Namely, r/R is a small expansion parameter, with $\boldsymbol{r}$ being the relative coordinate and $\boldsymbol{R}$ being the center-of-mass coordinate. For a compact bound state mostly dominated by the Coulomb core of the QCD interaction, as predicated by asymptotic freedom, the inverse relative coordinate is a scale of the order of typical relative momenta $1/r \sim p \sim m_h v$, which is integrated out by means of the multipole expansion. One arrives at the effective field theory called potential non-relativistic QCD (pNRQCD) [35], whose Wilson coefficients depend on the relative coordinate $\boldsymbol{r}$ (see, e.g., Ref. [15] for a review). The dynamical degrees of freedom of pNRQCD at the ultra-soft scale $E \sim \alpha_s/r \sim m_h v^2$ are bosonic color-singlet or -octet fields, S or O^a, as well as light degrees of freedom. The color-singlet and -octet fields explicitly couple to the ultra-soft chromoelectric fields through dipole interactions $\propto \boldsymbol{r} \cdot \boldsymbol{E}^a$ that are suppressed by one power of the relative coordinate. Some of the non-local Wilson coefficients play the role of the different contributions to the heavy quark-antiquark potential in QCD. However, there are non-potential contributions (i.e. terms that couple singlet- and octet-fields or different octet-fields among each other) that contribute as well in pNRQCD beyond the tree-level.

At leading order (LO), the attractive potential $V_s = -C_F \alpha_s/r$ of the singlet field S in pNRQCD is the *static potential* of QCD. Similarly, at this order the repulsive potential $V_o = +1/6\ \alpha_s/r$ of the octet field O^a is Coulombic, too. The singlet-singlet correlator in pNRQCD at leading order can be related to the Wilson loop in QCD by matching

$$W(r,t) = \langle \exp \mathrm{i}g \oint_{r\times t} dz^\mu A_\mu \rangle_{\mathrm{QCD}} = \langle S(r,0) S^\dagger(r,t) \rangle^{LO}_{\mathrm{pNRQCD}} \,. \tag{13}$$

It corresponds to quarkonia made from infinitely heavy constituents. In the vacuum, the large time behavior of the Wilson loop is given in terms of the ground state, the QCD static energy $E(r)$,

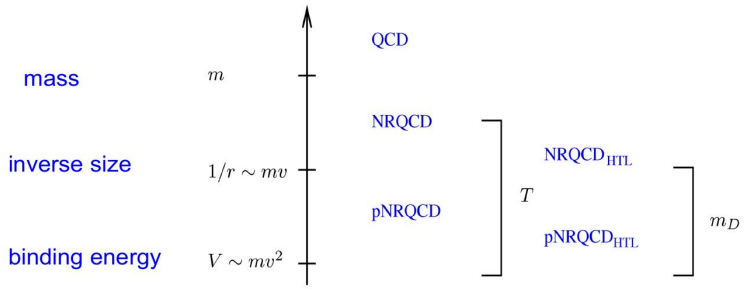

Figure 1: Relevant scale hierarchies for in-medium quarkonia.

$$E(r) = -\mathrm{i} \lim_{t\to\infty} \frac{\partial W(r,t)}{\partial t}, \tag{14}$$

which coincides with V_s at small enough distances. Such a stable ground state is represented by a distinct and well-separated delta function in the spectral function and would manifest as a plateau in the effective mass at sufficiently large imaginary time.

However, an unstable, quasiparticle excitation would feature locally in the spectral function as a regularized, (skewed) Breit-Wigner peak that is distinct and well-separated from other spectral features. Its skewing is due to the non-trivially time-dependent UV part of the correlator [36]. The tails of this Breit-Wigner peak would have to be regularized through the interplay between different states, or non-potential interactions with the medium that are not known in sufficient detail. While such a quasiparticle state cannot lead to a plateau in the effective mass at imaginary time (limited to $\tau < \beta$), the origin of the absence of a plateau in the effective mass is not immediately obvious. First, such absence could be caused even with a stable ground state by a time direction that is simply too short to permit decay of all excited states. Second, such absence could be caused by some quasiparticle remnant of the $T = 0$ ground state acquiring a finite width at $T > 0$, which cannot lead to a plateau as stated, while the right hand side in Eq. (14) might still become time independent. Third, such absence could be caused by a complete *melting* in the sense that there is no distinct quasiparticle remnant of the $T = 0$ ground state anymore. In the latter case, the right hand side in Eq. (14) would cease to be time-independent even in real time. Similar considerations apply with straightforward adaptations to finite mass quarkonia in a non-relativistic or relativistic formulation.

3.2 Weak-coupling approach

In the strict weak-coupling approach, the non-relativistic hierarchy $m_h \gg m_h v \gg m_h v^2$ is accompanied by a thermal hierarchy $\pi T \gg m_D \gg g^2 T$, where the Debye mass $m_D \sim gT$ is related to the scale of chromoelectric fields and $g^2 T$ to the scale of chromomagnetic fields. In both instances, the thermal coupling g is understood as a coupling at one of the two higher thermal scales.

Since the thermal coupling g or rather the ratio ${}^{m_D}/_{\pi T} \sim {}^{g}/_{\pi}$ is still large at temperatures far above the QCD transition, the convergence of perturbation theory for thermal observables is in many cases not obvious or even very poor in practice. Moreover, the magnetic scale $g^2 T$ is

inherently non-perturbative even at the highest temperatures, since the chromomagnetic fields are still subject to a confining three-dimensional SU(3) pure gauge theory. For these reasons, practical weak-coupling calculations are hampered in finite temperature QCD by the emergence of non-perturbative contributions from the chromomagnetic scale g^2T at some order, and by the need to resum contributions from the scale of the Debye mass.

Physically distinct regimes emerge depending on the relative ordering between the non-relativistic and thermal scales. The QCD static potential at finite temperature has been computed at leading order using the Hard Thermal Loop (HTL) approach. This calculation [37] identified a complex potential in the chromoelectric screening regime $1/r \sim m_D \ll \pi T$,

$$V_s^{\mathrm{HTL}}(r,T) = -C_F\alpha_s\left\{\frac{e^{-rm_D}}{r} + m_D + \mathrm{i}T\phi(rm_D)\right\}, \phi(x) = 2\int_0^\infty \frac{dz\, z}{(z^2+1)^2}\left\{1 - \frac{\sin(zx)}{zx}\right\}, \quad (15)$$

whose real part is Debye screened and coincides in this regime with the gauge-dependent singlet free energy (in Coulomb gauge) $F_S^{\mathrm{HTL}}(r,T) = -C_F\alpha_s\left\{\frac{e^{-rm_D}}{r} + m_D\right\}$ up to the order $O(g^4)$. Yet this result contains a non-trivial imaginary part as well, $\mathrm{Im}\, V_s^{\mathrm{HTL}}(r,T) = O(g^2T)$, that would vanish for $r \to 0$. Shortly after, this result was confirmed in a separate calculation [38] that also considered the short distance regime $\Delta V \sim \alpha_s/r \ll 1/r \ll m_D \ll \pi T$; in the latter regime the real part is vacuum-like without hints of screening,

$$V_s^{\mathrm{pNRQCD}}(r,T) = -\frac{C_F\alpha_s}{r} + r^2T^3\left\{O(g^4) + \mathrm{i}O\left(g^4, \frac{g^6}{(rT)^2}\right)\right\}, \quad (16)$$

while the imaginary part retains a non-zero value even as $r \to 0$.

As a consequence of these developments a new picture of quarkonia melting has begun to emerge. Namely, the presence of an imaginary part of the potential, which can be understood as being due to Landau damping and singlet-to-octet transitions, would lead to a dissociaton through decorrelation. Therefore, a dynamical picture of melting would replace the static picture suggested by Matsui and Satz [16]. Nevertheless, these weak-coupling results are unable to address questions concerning the relative importance of these different effects at phenomenologically interesting temperatures, i.e. in the broad crossover region and somewhat above, where the underlying assumption of a strictly weakly-coupled thermal scale hierarchy might be too optimistic.

3.3 Heavy quarkonia with relativistic quarks

One possible approach to tackle the question of heavy-quarkonia melting non-perturbativly – albeit in a qualitative manner – has been to study screening correlators on the lattice [39–41]. When studying temporal correlation functions in finite temperature lattice simulations one is generally hampered by having a very small number of data along the necessarily very short Euclidean time direction, since $aN_\tau = \beta$. Moreover, the matter is made worse by the symmetry of the relativistic correlator and kernel under $\tau \to \beta - \tau$, see Eq. (2), effectively reducing the amount of independent information by a factor two. As a consequence there are simply insufficient data for resolving subtle, temperature-induced changes of such a temporal correlator with lattices of the foreseeable future.

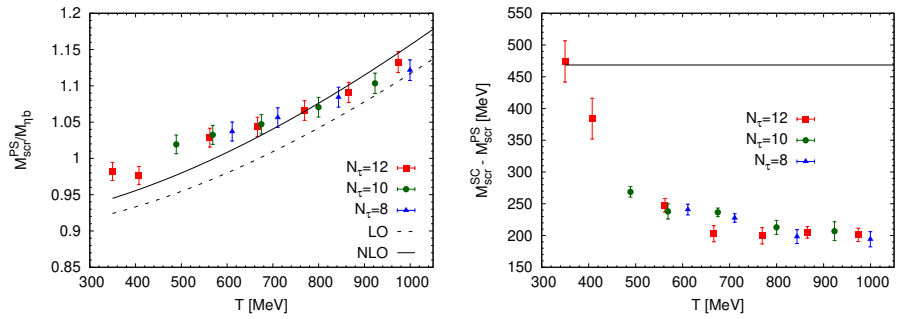

Figure 2: Masses of $T > 0$ bottomonia screening correlators using HISQ action in (2+1)-flavor QCD. The ratio $M(T)/M(0)$ in the pseudocsalar channel is consistent with 1 up to $T \approx 400\,\text{MeV}$ (left). The rapid drop of the difference of scalar and pseudoscalar masses from $T \approx 350\,\text{MeV}$ onward indicates the melting of χ_{b0}, but tampers out in a slow decrease due to heavy-quark mass effects (right). Figures from Ref. [42].

Moreover, since the kernel $K(\omega, \tau, \beta)$ for relativistic quarks in Eq. (2) has explicit temperature dependence, the temperature dependence of the correlator $G(\tau, T)$ does not originate only in the temperature dependence of the spectral function $\rho(\omega, T)$.

Considering instead a spatial or screening correlator has two advantages. First, the spatial extent of the lattice may be much larger than the inverse temperature – for a given lattice spacing a the number N_σ of data effectively decouples from N_τ. Second, the corresponding kernel has no explicit temperature dependence. Yet the price to pay is a more complicated relation between the screening correlator $G(z, T)$ (here in the z direction) and the underlying finite momentum spectral function $\rho(\omega, p_z, T)$, namely,

$$G(z,T) = \int_0^\beta d\tau \int d^2x_\perp \left\langle J(\tau, \boldsymbol{x}_\perp, z) J^\dagger(0) \right\rangle = \int_0^\infty \frac{2d\omega}{\omega} \int_{-\infty}^{\infty} dp_z e^{ip_z z} \rho(\omega, p_z, T) \overset{z\to\infty}{\sim} e^{-M(T)z}. \tag{17}$$

The exponential decay of a Euclidean quark-antiquark correlation function at large separations is independent of the direction between source and sink at zero temperature, or more generally speaking, whenever a stable mesonic ground state or a quasiparticle one with mostly unmodified properties exists. The effects of the different boundary conditions (periodic in space, antiperiodic in time) cancel as long as there is a stable meson [40]. Yet if there is no stable meson, but a non-interacting quark-antiquark pair, the screening mass is of the form $M(T) = \sum_i \sqrt{m_{h,i}^2 + (\pi T)^2}$ due to the anti-periodic boundary condition in time. When the ground state melts, the screening mass smoothly changes from its temperature-independent vacuum value $M_{\text{vac}} (= M_{\text{PDG}})$ to the asymptotic, temperature-dependent behavior of the non-interacting quark-antiquark pair.

Following these considerations, bottomonia screening correlators have been computed using the highly improved staggered quark (HISQ) action combined with the tree-level improved Symanzik gauge action on (2+1)-flavor QCD lattices close to the physical point ($m_l = m_s/20$, and a physical strange quark) [42] in an extension of an earlier study in the same HotQCD setup that had been focusing on open and hidden charm screening correlators [40]. This earlier study found that the

most compact ground state charmonia (J/Ψ and η_c) melt at temperatures higher than $T \gtrsim 200\,\text{MeV}$, while the more spatially extended χ_c states melt already slightly above the crossover. Hence, any charmonia have already been fully melted before they begin to contribute significantly to the equation of state beyond $T \gtrsim 300\,\text{MeV}$ as reported at this conference [43] for the HISQ action. The finite temperature lattices in the new study [42] had $N_\tau = 12,\ 10$, and 8, covering a temperature window of $T \sim [350, 1000]$ MeV. For the heavy-quark currents in Eq. (17) only local interpolating operators and point sources had been employed.

The main conclusions of this study are indicated in Fig. 2, and were reported together with many technical details at this conference [44]. Namely, the most compact ground state bottomonia ($\Upsilon(1S)$ and η_b) are mostly unmodified until at least $T \gtrsim 400\,\text{MeV}$, while the lowest, larger bottomonia (χ_{b0}, h_b) begin the melting already after $T \gtrsim 350\,\text{MeV}$. The qualitative modifications compared to charmonia screening correlators can be quantitatively understood in an effective field theory framework in terms of higher order corrections, since the onset of the naively expected high temperature behavior is suppressed by powers of T/m_b. Moreover, the staggered discretization artifacts were found to be commensurate with the size of other errors.

This program of studying screening correlators for $N_f = 3$ has been extended towards the electroweak scale using $O(a)$-improved Wilson fermions in the chiral limit. Due to mild cutoff effects precise continuum results could be obtained. These showed that deviations from the leading order – while being only a few percent down to $T \sim 1\,\text{GeV}$ – could not be captured quantitatively by the next-to-leading order even at $T \sim 80\,\text{GeV}$, and were reported at this conference [45]. Of course, these findings apply to heavy quarkonia as well at such high temperatures.

3.4 Heavy quarkonia using NRQCD

In general, the velocity v plays the role of an expansion parameter in NRQCD, which has been formulated on the lattice [46, 47], too. The computation of heavy-quark propagators simplifies to the solution of an initial value problem, since there is no backward propagating component. Suppressed higher order operator insertions as corrections to the identity alternate with propagation by one time step using the leading-order operator. This must be contrasted with the relativistic treatment, where obtaining a heavy-quark propagator requires a matrix inversion. Yet lattice NRQCD has one major drawback compared to a relativistic treatment or a treatment in the fully static limit. Namely, since it requires $m_h \gtrsim 1/a$, the continuum limit cannot be taken.

With regard to thermal correlators, these properties of NRQCD have two main consequences. First, for any given heavy-quark mass m_h and any N_τ, there is a rather strong upper limit on the temperatures to which it can be applied. This needs to be contrasted to relativistic formulations of heavy quarks, where there is a rather strong lower limit on the temperatures for which cutoff effects (parameterized via an expansion in am_h) are sufficiently small. Second, the inverse problem of reconstructing the spectral function from a thermal correlator such as the one in Eq. (1) is alleviated for any non-relativistic formulation. Any such formulation leads to a simplified, temperature-independent integral kernel, $e^{-\omega\tau}$, which is simply the kernel of a Laplace transform, and breaks the symmetry under $\tau \to \beta - \tau$, and thus effectively doubles the amount of independent information compared to the relativistic case, see Section 3.3.

In-medium NRQCD bottomonia have been studied for a long time by the FASTSUM collaboration [48] and through the well-established HotQCD setup [49–52]. One central difference in

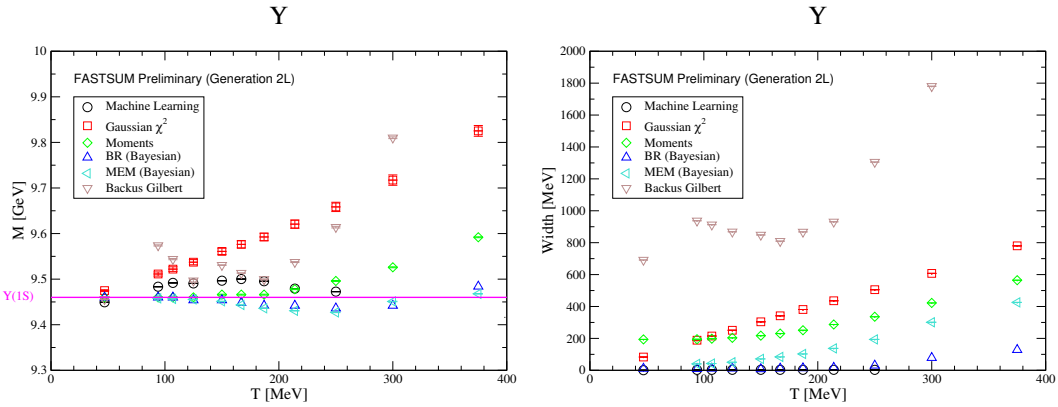

Figure 3: Upsilon correlators using NRQCD on gen. 2L FASTSUM lattices in (2+1)-flavor QCD. Different analysis methods may suggest opposite signs for the thermal mass shift (left). All analysis methods eventually find a finite width (monotonically increasing with temperature except for Backus-Gilbert method), although for some consistent with zero up to $T \lesssim 250\,\mathrm{MeV}$ (right). Figures courtesy of C. Allton.

the approaches of the two groups has been the temperature scan in a fixed scale approach (through variation of N_τ) of FASTSUM (most recent results on gen. 2L anisotropic lattices with (2+1) flavors of Wilson fermions, $m_\pi = 236\,\mathrm{MeV}$, ${}^{a_s}/_{a_t} = 3.45$) or through variation of the lattice spacing a in the HotQCD setup (HISQ/Tree action with $m_l = {}^{m_s}/_{20}$, see Section 3.3). A second key difference in the most recent studies is that FASTSUM has focused so far on the use of point sources for the NRQCD correlators, while HotQCD has established the use of extended sources.

The FASTSUM correlators obtained on the gen. 2L anisotropic lattices have been analyzed using a wide range of techniques – plain Gaussian χ^2 minimization, moments of the correlator, machine learning via Kernel Ridge Regression , the Backus-Gilbert method, and the two Bayesian approaches of Maximum Entropy Method (MEM) or Bayesian Reconstruction (BR). So far, a clear picture has not emerged yet; applied to the same correlators, the mass shifts may be positive or negative, and the widths do not reveal a pattern consistent between the various methods, as indicated in Fig. 3; preliminary results were discussed at this conference [53–55] and summarized in further conference proceedings [56].

The HotQCD results paint quite a different picture. An earlier analysis with point sources concluded that a plateau is not even reached in the pseudoscalar channel at $T = 0$ on fine lattices [49]. After accounting for this observation negative finite temperature mass shifts were identified. In order to overcome the lack of convergence to the ground state, they turned to Gaussian smeared sources that achieve a substantial suppression of the UV part of the correlator [50]. While extended sources distort the UV part, it was found that the distortion is very similar at $T = 0$ and at finite temperature. Therefore, as a key component of the HotQCD analysis the $T = 0$ UV part was subtracted from finite temperature correlators. Analyzing the $T = 0$ correlator with multi-exponential fits and subtracting the ground state contribution, the remnant was considered as the full UV part, and subtracted from the finite temperature correlator. In earlier calculations [57] a similar procedure had been already applied in the static limit, i.e. to Wilson loops. This UV subtraction produces an effective mass that is almost linear in τ at small times, namely $\tau \lesssim {}^{\beta}/_{2}$, but falls rapidly at $\tau \gtrsim {}^{\beta}/_{2}$.

On very general grounds, one may expect for any finite temperature spectral function $\rho_X(\omega, T)$

corresponding to a correlator with spatially extended interpolating fields that it exhibits three distinct features. First – unless it has reached the stage of complete melting – a well-separated, thermally-modified lowest spectral feature $\Omega_X(T)$, which could be traced back to the original $T = 0$ ground state. Second, a UV part due to excited states of the quark-antiquark pair immersed in the QCD medium. And third, a *low-energy tail* that is caused by excitations of the QCD medium itself that propagate backwards in imaginary time [58].

$$\rho_X(\omega,T) = \rho_X^{\Omega}(\omega,T) + \rho_X^{\mathrm{UV}}(\omega,T) + \rho_X^{\mathrm{tail}}(\omega,T). \tag{18}$$

These general considerations apply to any sufficiently extended operator, whether this is realized via NRQCD with smeared sources, or – as we will peruse later – Wilson loops. Since bottomonia vector correlators have a splitting of $m_{\Upsilon(2S)} - m_{\Upsilon(1S)} \sim 600\,\mathrm{MeV}$, one may assume sufficient separation at least for $\Upsilon(1S)$ at low temperatures. The UV subtracted correlators correspond to $\rho_X^{\mathrm{UV}}(\omega,T) - \rho_X^{\mathrm{UV}}(\omega,0) \approx 0$, while rapid falloff at large $\tau \gtrsim \beta/2$ originates in $\rho_X^{\mathrm{tail}}(\omega,T)$. Taking these features into account, the authors analyzed the subtracted correlators through fits of the form

$$G^{\mathrm{sub}}(\tau,T) = A^{\Omega}(T) e^{-\Omega(T)\tau + (\Gamma^G(T))^2 \frac{\tau^2}{2}} + A^{\mathrm{tail}}(T) e^{-\omega^{\mathrm{tail}}(T)\tau}, \quad \omega^{\mathrm{tail}}(T) \ll \Omega(T). \tag{19}$$

While Eq. (19) does not correspond to the Breit-Wigner shape that is necessary in the quasi-particle picture, it can be understood as a regularization of a Breit-Wigner peak through a Gaussian. The width $\Gamma^G(T)$ of the Gaussian then has to be rescaled to the corresponding effective width $\Gamma(T) = \sqrt{2\ln 2}\Gamma^G(T)$ of the Breit-Wigner that it imitates. Since the extended correlators do not provide sufficient number of independent data over a wide enough range of τ, further features such as skewing (cf. Section 3.1) could not be resolved so far. Moreover, for the same reason the low-energy tail was modeled as a delta function. This analysis found a thermal mass shift for the $\Upsilon(1S)$ that is almost negligible, while its thermal width increases monotonically with the temperature [50].

With approximate eigenfunctions of a Cornell potential used as interpolating fields when solving a GEVP, similar findings were obtained even for the first few excited states [51], with similarly small mass shifts, but significantly larger widths. The authors went one step further, and solved the Schrödinger equation for the $T = 0$ lattice NBS amplitudes

$$\left\{ -\frac{\Delta}{2m_b} + V(r) \right\} \phi_{\Upsilon(\mathrm{nS})} = E_{\Upsilon(\mathrm{nS})} \phi_{\Upsilon(\mathrm{nS})} \tag{20}$$

using two different energy levels to determine the effective bottom quark mass and reconstruct the underlying potential. This potential was found to be quantitatively consistent with the one obtained from Wilson loops. Extending the approach of NBS amplitudes to finite temperature, the authors found minimal temperature dependence of the BS amplitudes $\phi_{\Upsilon(\mathrm{nS})}$ at small τ, but a substantial τ dependence for the NBS amplitudes of the excited states [52].

The NBS amplitudes $\phi_{\Upsilon(\mathrm{nS})}$ of Ref. [52] were processed in a deep neural network (DNN) [59] solving Eq. (20) to address the question whether the specific fit form in Eq. (19) may have led to substantial bias in Refs. [50, 51]. The DNN results positively confirmed the earlier calculation. Another fully independent calculation of the quark-antiquark potential by the FASTSUM collaboration employing lattice NBS amplitudes when solving Eq. (20) was reported at this conference [60], too.

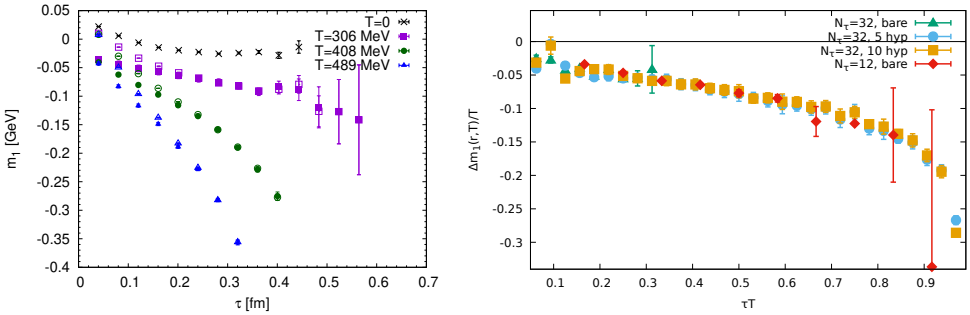

Figure 4: Wilson line correlators in Coulomb gauge in (2+1)-flavor QCD. Correlators with smaller N_τ exhibit stronger τ dependence at large τ, and lack the plateau present at $T = 0$. Subtraction of the vacuum UV part (filled symbols) reveals an approximately linear decrease until $\tau \gtrsim \beta/2$ (left, from [58]). We see smearing independence as well as consistency with results obtained on coarser lattices at large enough τT to be accessible by the latter. Smaller τT values seem to suffer from major fluctuations due to large cancellations that become prominent after the subtraction of the large $T = 0$ UV part (right).

3.5 Heavy quarkonia using static quarks

In the following, we leave any finite heavy-quark mass behind and consider the static limit, which inherits from the NRQCD case the lack of symmetry under $\tau \to \beta - \tau$ and the simple Laplace kernel in the relation between correlator and spectral function in Eq. (1). We define cumulants of the Wilson loop $W(r,T,\tau)$ (or, more generally, of any correlator $G(T,\tau)$) as

$$m_1(r,T,\tau) = -\frac{\partial \ln W(r,T,\tau)}{\partial \tau}, \quad m_{n+1}(r,T,\tau) = \frac{\partial m_n(r,T,\tau)}{\partial \tau} \quad \text{for } n > 1. \tag{21}$$

If m_1 is defined through a discrete derivative, e.g. the logarithm of a next-neighbor ratio, it coincides with the usual effective mass $m_1(r,T,\tau) = {}^1/_a \ln\left[{}^{W(r,T,\tau)}/_{W(r,T,\tau+a)}\right]$. For the analysis of the Wilson loops – which all represent extended operators – the same technique of subtracting the vacuum UV part as in the NRQCD case has been applied, cf. Section 3.4. Results for $T = 0$ or three different temperatures are shown in Fig. 4, where the simplified τ dependence of the subtracted correlators at $\tau \lesssim \beta/2$ is evident. This study used the well-established HotQCD setup (HISQ/Tree action with $m_l = {}^{m_s}/_{20}$, see Section 3.3), too.

Instead of a rectangular Wilson loop, the authors considered the correlator of two temporal Wilson lines in Coulomb gauge, or a Wilson loop with spatially smeared (three-dimensional HYP smearing [61]) spatial Wilson lines. It was demonstrated at $T = 0$ [62] that the smearing reduces the UV part of the correlator, and at $T > 0$ [58] that the smeared Wilson loops and Coulomb gauge Wilson line correlators are – after appropriate subtraction of the respective vacuum UV parts – statistically consistent in the range of approximately linear τ dependence, namely at $\tau \lesssim \beta/2$, but differ in their rapid falloff at $\tau \gtrsim \beta/2$ that is related to the low-energy tail. Hence, the behavior at $\tau \lesssim \beta/2$ may be understood as independent of the details of the interpolating operator. This strongly points toward the existence of a quasiparticle state.

On the one hand, an approximately linear τ dependence of $m_1(r,T,\tau)$ for the UV-subtracted correlator implies nearly constant $m_2(r,T,\tau)$, and approximately zero $m_3(r,T,\tau)$ at $\tau \lesssim \beta/2$. On the other hand, the steep falloff at $\tau \gtrsim \beta/2$ implies that $m_2(r,T,\tau)$ becomes increasingly negative.

This indicates negative $m_3(r,T,\tau)$ as well. So far, the correlators with $N_\tau \leq 16$ did not provide sufficient resolution for more than the first three cumulants; $m_3(r,T,\tau)$ could be determined only for $T > 300\,\text{MeV}$ [58]. While most of the analysis focused on finite temperature lattices with $N_\tau = 12$ close to the physical point ($m_l = {}^{m_s}/_{20}$, and a physical strange quark), the comparison to results with $N_\tau = 16$ or 10 suggests mild cutoff effects. Juxtaposition with results for $m_l = {}^{m_s}/_{5}$ at $T \gtrsim 500\,\text{MeV}$ suggests a mild quark-mass dependence (at high temperatures) as naively expected.

In order to achieve a resolution of the higher cumulants capable of resolving an imprint of the non-trivial dynamics of the quasiparticle state, the HotQCD collaboration has commenced exploratory studies of Wilson line correlators in Coulomb gauge on exceptionally fine lattices $a \approx 0.028\,\text{fm}$ using $N_\tau = 32$ or 24, i.e. in a fixed scale approach. In this study, the subtraction of the UV part – previously implemented in terms of fits to the $T = 0$ correlator – was substituted by a direct calculation of the ratio between two correlators at different temperatures. The new approach yields in all studied cases statistically consistent results; the first cumulant of the ratio is the difference between first cumulants at the two different temperatures, i.e. $\Delta m_1(r,T) = m_1(r,T) - m_1(r,0)$, see Fig. 4. Preliminary results have been reported at this conference [63]. Use of such fine lattices necessitated noise suppression techniques to obtain a good signal at intermediate to large τ even for quite small distances. The use of four-dimensional HYP smearing [61] after Coulomb gauge fixing, which had been introduced for studying the screening masses of Polyakov loop correlators at large distances [64, 65] is being used as a noise suppresion technique on these fine lattices as well. While the UV part cancels very well between smeared $T = 0$ and finite temperature correlators, previously insignificant statistical fluctuations seem to become prominent due to the cancellations. For this reason, conclusive results on higher cumulants at $\tau \lesssim {}^{\beta}/_{2}$ may require improved statistics.

A similar reasoning as in the non-relativstic case means that the fit in Eq. (19) could be applied to the UV subtracted Wilson loops as well. These fits have been reported at this conference [66], and suggest a strong-binding scenario, where the position of the lowest spectral feature $\Omega(r,T)$ is practically independent of the temperature, while the corresponding effective width $\Gamma(r,T)$ shows naive scaling ${}^{\Gamma(rT)}/_{T} = f(rT)$ for all temperatures down to the crossover. An alternative analysis following a different approach – reported in Ref. [66], too – also suggests a strong-binding scenario, where the position of the lowest spectral feature $\Omega(r,T)$ is nearly independent of the temperature, while the corresponding width $\Gamma(r,T)$ shows weaker than naive scaling with T and rT. In this approach the Matsubara correlator at tree-level improved frequencies is obtained as the Fourier transform of the Euclidean-time correlator. Then the Matsubara correlator is interpolated using Padé approximants, and finally analytically continued from imaginary to real frequencies, where the properties of the lowest spectral feature could be read off directly. The third approach discussed in Ref. [66] is a Bayesian one, where the Bayesian Reconstruction (BR) [67] was applied as a regulator in the analysis of the Wilson loops. However, the very precise underlying lattice correlators on ensembles in the HotQCD setup are explicitly sensitive to tiny positivity violations at $r \sim a$ and $\tau \sim a$ due to the use of the improved gauge action; these can be resolved only on fine lattices [62]. Hence, the BR analysis was limited to sufficiently coarse lattices, namely for $N_\tau = 12$ just at the crossover, where the BR method is consistent with the other results.

Earlier Padé or BR analyses on subsets of these data without some of the recent refinements of the analysis (for details, see Ref. [58]) found within large errors somewhat better support for the weak-binding picture [68], similar to an earlier analysis using the quenched approximation or

(2+1)-flavor lattice QCD with an AsqTad sea [69].

The leading-order HTL result in Eq. (15) could be a very suggestive inspiration for an analysis of the finite temperature Wilson loops on the lattice, since it contains a regularized Breit-Wigner peak. Such an approach had been followed in the past by fitting Wilson loops on the lattice with a rescaled form of this result [70]. However, before one embarks on such an endeavor, it is cautious to discern to which extent the lattice Wilson loops share characteristic features of the leading-order HTL result, as reported at this conference [66]. The first cumulant of the correlator reconstructed from the HTL spectral function,

$$m_1^{\mathrm{HTL}}(r,\tau) = \mathrm{Re}\, V_s^{\mathrm{HTL}}(r,T) + \frac{\mathrm{Im}\, V_s^{\mathrm{HTL}}(r,T)\beta}{\pi} \frac{\partial \ln \sin\left(\pi \frac{\tau}{\beta}\right)}{\partial \tau}, \quad \text{for } \tau \sim \frac{\beta}{2}, \tag{22}$$

is antisymmetric under $\tau \longrightarrow \beta - \tau$, and its midpoint value at $\tau = \beta/2$ is the real part $\mathrm{Re}\, V_s^{\mathrm{HTL}}(r,T)$, which coincides at the leading order with the singlet free energy in Coulomb gauge $F_S^{\mathrm{HTL}}(r,T)$. A divergence-free comparison is possible in terms of $\mathrm{Re}\, V_s(r,T) - F_S(r,T)$, since both share the same renormalon in the weak-coupling expansion or $1/a$ divergence in the lattice scheme. Due to the lack of a significant UV contribution in the HTL spectral function, however, juxtaposing the HTL expression with the lattice should be done in terms of the UV-subtracted data. First, the characteristic antisymmetry is not represented in the lattice data over a large range in τ. Second, the decrease of the lattice data is much steeper than in HTL. Third, the midpoint value of the lattice result is only at very high temperatures $T \sim 2\,\mathrm{GeV}$ consistent with zero (the HTL prediction); see Refs. [58, 66] for further details.

Nonetheless, with a fit range limited to a narrow interval around the midpoint $\tau = \beta/2$, it is legitimate to analyze the lattice Wilson loops using Eq. (22) in a discretized form and obtain predictions for $\Omega \sim \mathrm{Re}\, V_s$ and $\Gamma \sim \mathrm{Im}\, V_s$. In the past such an HTL-inspired analysis had been applied to spatially-smeared Wilson loops on anisotropic lattices in the quenched approximation [71]. The results from such an analysis of the (2+1)-flavor QCD data in the HotQCD setup have been reported at this conference [72]. This analysis suggests a weak-binding scenario, where the position of the lowest spectral feature $\Omega(r,T)$ is quantitatively close to $F_S(r,T)$, while the corresponding width $\Gamma(r,T)$ shows weaker than naive scaling. In particular, $\Omega(r,T)$ stays close to $F_S(r,T)$ for $T > 300\,\mathrm{MeV}$ much beyond $rT \lesssim 0.3$ where similar agreement has been observed for the $T = 0$ static energy as well [12]. These findings are similar to the earlier ones in the quenched approximation [71].

All recently applied lattice analysis methods suggest that the finite temperature Wilson loop exhibits a well-defined lowest spectral feature $\Omega(r,T)$ at $r \lesssim 1.5/T$ and up to $T \sim 2\,\mathrm{GeV}$, which can be considered as a complex, quasiparticle remnant of the $T = 0$ static energy. All the methods robustly point towards a significant width of this spectral feature – or in other words to a large imaginary part of the complex static energy. This width grows for increasing r or increasing temperature, but can be seen already at the crossover. However, at present static quark-antiquark correlators do not provide a conclusive picture on the question of weak- vs strong-binding scenario yet. The expected screening of the real part of the static energy is not evident in our calculations.

3.6 Heavy quarkonia free energies

The free energies of heavy quarkonia can be studied by evaluating the thermal static quark-antiquark correlators at $\tau = \beta$, i.e., in a gauge-invariant manner in terms of the Polyakov loop correlator

$$C_P(r,T) = \langle P(0)P^\dagger(\boldsymbol{r})\rangle\,, \tag{23}$$

with $P(\boldsymbol{r}) = \langle \mathrm{Re\,Tr} U(\beta,\boldsymbol{r})\rangle$ being the trace of the Polyakov loop. After renormalization $C_P(r,T) = e^{-F_{q\bar{q}}(r,T)/T}$. For $r \ll \beta$ this correlator can be expressed in terms of the $T = 0$ singlet- or octet-potentials and the adjoint Polyakov loop; substituting the static energy on the lattice instead of the potentials and accounting for Casimir scaling violations, good agreement up $rT \lesssim 0.35$ suggests that within such distances no thermal modification occurs besides the changes of the adjoint Polyakov loop [12]. The increasing value of the adjoint Polyakov loop implies that color-octet states – dissociated static quarkonia – become less suppressed.

At large distances, $C_P(r,T) = C_P^R(r,T) + C_P^I(r,T)$ can be understood as the sum of contributions from the real or imaginary parts of the Polyakov loops, while it asymptotes at $\langle P\rangle^2$ in the large distance limit. Their ratio

$$C_P^R(r,T) = \langle \mathrm{Re}\,P(0)\mathrm{Re}\,P^\dagger(\boldsymbol{r})\rangle\,, \quad C_P^I(r,T) = \langle \mathrm{Im}\,P(0)\mathrm{Im}\,P^\dagger(\boldsymbol{r})\rangle\,, \tag{24}$$

where $C_P^R(r,T)$ is dominated by two-gluon exchange, while $C_P^I(r,T)$ is dominated by three-gluon exchange. Asymptotically, the normalized correlators

$$\widetilde{C}_P^R(r,T) = \frac{\langle \mathrm{Re}\,P(0)\mathrm{Re}\,P^\dagger(\boldsymbol{r})\rangle - \langle P\rangle^2}{\langle P\rangle^2}, \quad \widetilde{C}_P^I(r,T) = \frac{\langle \mathrm{Im}\,P(0)\mathrm{Im}\,P^\dagger(\boldsymbol{r})\rangle}{\langle P\rangle^2}, \tag{25}$$

decay as $\widetilde{C}_P^{R,I}(r,T) \propto {}^{e^{m_{R,I}r}}\!/_{rT}$ with screening masses $m_{R,I}$. At leading order, these screening masses satisfy $m_R = 2m_D, m_I = 3m_D$; above the crossover region temperature they are proportional to the temperature up to subleading, logarithmic corrections.

Computing the Polyakov loop correlators at large distances is challenging due to the poor signal-to-noise ratio. However, using four-dimensional hypercubic smearing [61] a good signal can be obtained up to $r \sim \beta$ in the HotQCD setup (see Sec. 3.3), which is sufficient to determine the screening masses ${}^{m_R}\!/_T \simeq 4.5$ and ${}^{m_I}\!/_T \simeq 8$ over the temperature range $(170 - 1500)$ MeV that were reported at this conference [65]. These results are quantitatively consistent with earlier calculations in full QCD [73] or in dimensionally reduced effective field theory [74]. The corresponding screening length ${}^1\!/_{m_D} \simeq {}^2\!/_{m_R} \simeq {}^3\!/_{m_I}$ is $(0.38 - 0.44)/T$, which would suggest melting temperatures due to screening of about 380 MeV or 190 MeV for $\Upsilon(1S)$ or J/Ψ, respectively.

4. Conclusions

In these proceedings, we have reviewed the recent advances in lattice gauge theory with respect to the non-pertubative calculation of in-medium heavy-quark observables at finite temperature. We

have inspected two different, but interrelated problems – isolated heavy quarks that are subject to dynamical *transport phenomena*, and quarkonia, i.e., correlated heavy quark-antiquark pairs, that are subject to dynamical *melting*. The dynamical nature of both phenomena implies that the ill-posed inverse problem in Eq. (1) needs to be solved.

The key observables for heavy-quark transport are chromo-electric and -magnetic field-strength correlators, which require efficient noise suppression techniques and have been limited so far to the quenched approximation. Recently, they have been determined using the gradient flow instead of the multi-level algorithm for the noise reduction as reported at this conference [31, 32]. This alleviates issues with renormalization in previous calculations, and opens up the prospect of obtaining the first non-perturbative QCD results in the near future.

The key observables for in-medium heavy quarkonia are either spatial or temporal quarkonia correlators, or thermal Wilson loops, which have been studied with three dynamical flavors by multiple groups. Spatial bottomonia correlators have been computed [42] with HISQ action in an extension of a previous study in the charm sector [40]. Both studies support the expected melting temperatures of a strong-binding scenario as reported at this conference [44]. Preliminary results from a study of spatial correlators in the chiral limit were reported at this conference [45], which determined that the next-to-leading order does not quantitatively capture the percent-level deviation between the leading order and the lattice even at the electroweak scale. Of course, these findings apply to heavy quarkonia as well. Temporal bottomonia correlators have been computed using NRQCD by the FASTSUM and HotQCD collaborations. The HotQCD results [50–52, 59] using extended sources generally support the strong-binding scenario. Older results from FASTSUM [48] or HotQCD [49] as well as preliminary FASTSUM results [53–56, 60] with local point sources paint a less conclusive picture. Thermal Wilson loops or Coulomb gauge Wilson line correlators have been analyzed by the HotQCD collaboration [58]. These calculations robustly point to the existence of a well-separated, lowest spectral structure with a finite width as the remnant of the $T = 0$ static energy, but are inconclusive with regard to the weak- or strong-binding scenarios. Some calculations using the same data were reported at this conference, which supported for an HTL-inspired Ansatz the weak-binding [72], or for model fits or Padé analysis the strong-binding scenario [66]. The screening length obtained from Polyakov correlators would suggest melting temperatures closer to a strong-binding scenario [65]. In this regard it is not obvious how this result, together with the robust evidence for the finite thermal width, and the melting patterns from the spatial quarkonia correlators can be reconciled in a consistent picture. The most likely path towards a more conclusive result is the use of very fine lattices that could exclude some solutions of the inverse problem; preliminary results in this direction from the HotQCD collaboration have been reported at this conference [63]. Of course, the required fine ensembles would be valuable for calculation of spatial or temporal quarkonia correlators, or for the field-strength correlators from which transport coefficients are determined.

Acknowledgments

We thank P. Petreczky for discussions, careful reading and comments on the manuscript. J.H.W.'s research was funded by the Deutsche Forschungsgemeinschaft (DFG, German Research Foundation) - Projektnummer 417533893/GRK2575 "Rethinking Quantum Field Theory".

References

[1] Y. Akiba, A. Angerami, H. Caines, A. Frawley, U. Heinz, B. Jacak, J. Jia, T. Lappi, W. Li and A. Majumder, *et al.* [arXiv:1502.02730 [nucl-ex]].

[2] H. T. Ding, F. Karsch and S. Mukherjee, doi:10.1142/9789814663717_0001.

[3] A. Bazavov *et al.* [USQCD], Eur. Phys. J. A **55**, no.11, 194 (2019) [arXiv:1904.09951 [hep-lat]].

[4] A. Bazavov and J. H. Weber, Prog. Part. Nucl. Phys. **116**, 103823 (2021) [arXiv:2010.01873 [hep-lat]].

[5] D. J. Gross, R. D. Pisarski and L. G. Yaffe, Rev. Mod. Phys. **53**, 43 (1981).

[6] F. Karsch, K. Redlich and A. Tawfik, Eur. Phys. J. C **29**, 549-556 (2003) [arXiv:hep-ph/0303108 [hep-ph]].

[7] R. Hagedorn, Nuovo Cim. Suppl. **3**, 147-186 (1965) CERN-TH-520.

[8] N. Cabibbo and G. Parisi, Phys. Lett. B **59**, 67-69 (1975).

[9] H. T. Ding *et al.* [HotQCD], Phys. Rev. Lett. **123**, no.6, 062002 (2019) [arXiv:1903.04801 [hep-lat]].

[10] A. Bazavov *et al.* [HotQCD], Phys. Lett. B **795**, 15-21 (2019) [arXiv:1812.08235 [hep-lat]].

[11] S. Borsanyi, Z. Fodor, J. N. Guenther, R. Kara, S. D. Katz, P. Parotto, A. Pasztor, C. Ratti and K. K. Szabo, Phys. Rev. Lett. **125**, no.5, 052001 (2020) [arXiv:2002.02821 [hep-lat]].

[12] A. Bazavov *et al.* [TUMQCD], Phys. Rev. D **98**, no.5, 054511 (2018) [arXiv:1804.10600 [hep-lat]].

[13] N. Brambilla, S. Eidelman, B. K. Heltsley, R. Vogt, G. T. Bodwin, E. Eichten, A. D. Frawley, A. B. Meyer, R. E. Mitchell and V. Papadimitriou, *et al.* Eur. Phys. J. C **71**, 1534 (2011) [arXiv:1010.5827 [hep-ph]].

[14] A. Rothkopf, Phys. Rept. **858**, 1-117 (2020) [arXiv:1912.02253 [hep-ph]].

[15] N. Brambilla, A. Pineda, J. Soto and A. Vairo, Rev. Mod. Phys. **77**, 1423 (2005) [arXiv:hep-ph/0410047 [hep-ph]].

[16] T. Matsui and H. Satz, Phys. Lett. B **178**, 416-422 (1986).

[17] F. Karsch, D. Kharzeev and H. Satz, Phys. Lett. B **637**, 75-80 (2006) [arXiv:hep-ph/0512239 [hep-ph]].

[18] B. Svetitsky, Phys. Rev. D **37**, 2484-2491 (1988).

[19] H. B. Meyer, New J. Phys. **13**, 035008 (2011) [arXiv:1012.0234 [hep-lat]].

[20] D. Banerjee, S. Datta, R. Gavai and P. Majumdar, Phys. Rev. D **85**, 014510 (2012) [arXiv:1109.5738 [hep-lat]].

[21] A. Francis, O. Kaczmarek, M. Laine, T. Neuhaus and H. Ohno, Phys. Rev. D **92**, no.11, 116003 (2015) [arXiv:1508.04543 [hep-lat]].

[22] N. Brambilla, V. Leino, P. Petreczky and A. Vairo, Phys. Rev. D **102**, no.7, 074503 (2020) [arXiv:2007.10078 [hep-lat]].

[23] R. Rapp and H. van Hees, [arXiv:0903.1096 [hep-ph]].

[24] M. Laine, JHEP **04**, 124 (2011) [arXiv:1103.0372 [hep-ph]].

[25] C. P. Herzog, A. Karch, P. Kovtun, C. Kozcaz and L. G. Yaffe, JHEP **07**, 013 (2006) [arXiv:hep-th/0605158 [hep-th]].

[26] A. Bouttefeux and M. Laine, JHEP **12**, 150 (2020) doi:10.1007/JHEP12(2020)150 [arXiv:2010.07316 [hep-ph]].

[27] S. Caron-Huot, M. Laine and G. D. Moore, JHEP **04**, 053 (2009) [arXiv:0901.1195 [hep-lat]].

[28] C. Christensen and M. Laine, Phys. Lett. B **755**, 316-323 (2016) [arXiv:1601.01573 [hep-lat]].

[29] M. Lüscher, JHEP **08**, 071 (2010) [erratum: JHEP **03**, 092 (2014)] [arXiv:1006.4518 [hep-lat]].

[30] L. Altenkort, A. M. Eller, O. Kaczmarek, L. Mazur, G. D. Moore and H. T. Shu, Phys. Rev. D **103**, no.1, 014511 (2021) [arXiv:2009.13553 [hep-lat]].

[31] J. Mayer-Steudte, N. Brambilla, V. Leino and P. Petreczky, [arXiv:2111.10340 [hep-lat]].

[32] L. Altenkort, A. M. Eller, O. Kaczmarek, L. Mazur, G. D. Moore and H. T. Shu, [arXiv:2111.12462 [hep-lat]].

[33] N. Brambilla, M. A. Escobedo, A. Vairo and P. Vander Griend, Phys. Rev. D **100**, no.5, 054025 (2019) [arXiv:1903.08063 [hep-ph]].

[34] A. Manohar and H. Georgi, Nucl. Phys. B **234**, 189-212 (1984).

[35] N. Brambilla, A. Pineda, J. Soto and A. Vairo, Nucl. Phys. B **566**, 275 (2000) [arXiv:hep-ph/9907240 [hep-ph]].

[36] Y. Burnier and A. Rothkopf, Phys. Rev. D **86**, 051503 (2012) [arXiv:1208.1899 [hep-ph]].

[37] M. Laine, O. Philipsen, P. Romatschke and M. Tassler, JHEP **03**, 054 (2007) [arXiv:hep-ph/0611300 [hep-ph]].

[38] N. Brambilla, J. Ghiglieri, A. Vairo and P. Petreczky, Phys. Rev. D **78**, 014017 (2008) [arXiv:0804.0993 [hep-ph]].

[39] F. Karsch, E. Laermann, S. Mukherjee and P. Petreczky, Phys. Rev. D **85**, 114501 (2012) [arXiv:1203.3770 [hep-lat]].

[40] A. Bazavov, F. Karsch, Y. Maezawa, S. Mukherjee and P. Petreczky, Phys. Rev. D **91**, no.5, 054503 (2015) [arXiv:1411.3018 [hep-lat]].

[41] A. Bazavov, S. Dentinger, H. T. Ding, P. Hegde, O. Kaczmarek, F. Karsch, E. Laermann, A. Lahiri, S. Mukherjee and H. Ohno, *et al.* Phys. Rev. D **100**, no.9, 094510 (2019) [arXiv:1908.09552 [hep-lat]].

[42] P. Petreczky, S. Sharma and J. H. Weber, Phys. Rev. D **104**, no.5, 054511 (2021) [arXiv:2107.11368 [hep-lat]].

[43] J. H. Weber, A. Bazavov and P. Petreczky, PoS **LATTICE2021**, 060 (2021) [arXiv:2110.03606 [hep-lat]].

[44] P. Petreczky, S. Sharma and J. H. Weber, [arXiv:2112.07043 [hep-lat]].

[45] D. Laudicina, et al., PoS(LATTICE2021) 190.

[46] B. A. Thacker and G. P. Lepage, Phys. Rev. D **43**, 196-208 (1991).

[47] G. P. Lepage, L. Magnea, C. Nakhleh, U. Magnea and K. Hornbostel, Phys. Rev. D **46**, 4052-4067 (1992) [arXiv:hep-lat/9205007 [hep-lat]].

[48] G. Aarts, C. Allton, T. Harris, S. Kim, M. P. Lombardo, S. M. Ryan and J. I. Skullerud, JHEP **07**, 097 (2014) [arXiv:1402.6210 [hep-lat]].

[49] S. Kim, P. Petreczky and A. Rothkopf, JHEP **11**, 088 (2018) [arXiv:1808.08781 [hep-lat]].

[50] R. Larsen, S. Meinel, S. Mukherjee and P. Petreczky, Phys. Rev. D **100**, no.7, 074506 (2019) [arXiv:1908.08437 [hep-lat]].

[51] R. Larsen, S. Meinel, S. Mukherjee and P. Petreczky, Phys. Lett. B **800**, 135119 (2020) [arXiv:1910.07374 [hep-lat]].

[52] R. Larsen, S. Meinel, S. Mukherjee and P. Petreczky, Phys. Rev. D **102**, 114508 (2020) [arXiv:2008.00100 [hep-lat]].

[53] T. Spriggs, G. Aarts, C. Allton, T. Burns, B. Jäger, S. Kim, M. P. Lombardo, S. Offler, B. Page and S. M. Ryan, *et al.* [arXiv:2112.01599 [hep-lat]].

[54] B. Page, G. Aarts, C. Allton, B. Jäger, S. Kim, M. P. Lombardo, S. Offler, S. M. Ryan, J. I. Skullerud and T. Spriggs, [arXiv:2112.02075 [hep-lat]].

[55] S. Offler, G. Aarts, C. Allton, B. Jäger, S. Kim, M. P. Lombardo, B. Page, S. M. Ryan, J. I. Skullerud and T. Spriggs, [arXiv:2112.02116 [hep-lat]].

[56] T. Spriggs, G. Aarts, C. Allton, T. Burns, R. H. D'Arcy, B. Jäger, S. Kim, M. P. Lombardo, S. Offler and B. Page, *et al.* [arXiv:2112.04201 [hep-lat]].

[57] P. Petreczky *et al.* [TUMQCD], Nucl. Phys. A **967**, 592-595 (2017) [arXiv:1704.08573 [hep-lat]].

[58] D. Bala, O. Kaczmarek, R. Larsen, S. Mukherjee, G. Parkar, P. Petreczky, A. Rothkopf and J. H. Weber, [arXiv:2110.11659 [hep-lat]].

[59] S. Shi, K. Zhou, J. Zhao, S. Mukherjee and P. Zhuang, [arXiv:2105.07862 [hep-ph]].

[60] T. Spriggs, C. Allton, T. Burns and S. Kim, [arXiv:2112.09092 [hep-lat]].

[61] A. Hasenfratz and F. Knechtli, Phys. Rev. D **64**, 034504 (2001) [arXiv:hep-lat/0103029 [hep-lat]].

[62] A. Bazavov *et al.* [TUMQCD], Phys. Rev. D **100**, no.11, 114511 (2019) [arXiv:1907.11747 [hep-lat]].

[63] D. Hoying, A. Bazavov, D. Bala, G. Parkar, O. Kaczmarek, R. Larsen, S. Mukherjee, P. Petreczky, A. Rothkopf and J. H. Weber, [arXiv:2110.00565 [hep-lat]].

[64] S. Steinbeißer *et al.* [TUMQCD], PoS **Confinement2018**, 266 (2018) [arXiv:1811.12846 [hep-lat]].

[65] P. Petreczky, S. Steinbeißer and J. H. Weber, [arXiv:2112.00788 [hep-lat]].

[66] G. Parkar, D. Bala, O. Kaczmarek, R. Larsen, S. Mukherjee, P. Petreczky, A. Rothkopf and J. H. Weber, [arXiv:2111.15437 [hep-lat]].

[67] Y. Burnier and A. Rothkopf, Phys. Rev. Lett. **111**, 182003 (2013) [arXiv:1307.6106 [hep-lat]].

[68] P. Petreczky, A. Rothkopf and J. Weber, Nucl. Phys. A **982**, 735-738 (2019) [arXiv:1810.02230 [hep-lat]].

[69] Y. Burnier, O. Kaczmarek and A. Rothkopf, Phys. Rev. Lett. **114**, no.8, 082001 (2015) [arXiv:1410.2546 [hep-lat]].

[70] A. Bazavov, Y. Burnier and P. Petreczky, Nucl. Phys. A **932**, 117-121 (2014) [arXiv:1404.4267 [hep-lat]].

[71] D. Bala and S. Datta, Phys. Rev. D **101**, no.3, 034507 (2020) [arXiv:1909.10548 [hep-lat]].

[72] D. Bala, O. Kaczmarek, R. Larsen, S. Mukherjee, G. Parkar, P. Petreczky, A. Rothkopf and J. H. Weber, [arXiv:2112.00664 [hep-lat]].

[73] S. Borsányi, Z. Fodor, S. D. Katz, A. Pásztor, K. K. Szabó and C. Török, JHEP **04**, 138 (2015) [arXiv:1501.02173 [hep-lat]].

[74] A. Hart, M. Laine and O. Philipsen, Nucl. Phys. B **586**, 443-474 (2000) [arXiv:hep-ph/0004060 [hep-ph]].